Science Advances
AAAS

advances.sciencemag.org/cgi/content/full/6/20/eaay3188/DC1

Supplementary Materials for

Climate-driven aerobic habitat loss in the California Current System

Evan M. Howard*, Justin L. Penn, Hartmut Frenzel, Brad A. Seibel, Daniele Bianchi, Lionel Renault, Fayçal Kessouri, Martha A. Sutula, James C. McWilliams, Curtis Deutsch*

*Corresponding author. Email: ehoward2@uw.edu (E.M.H.); cdeutsch@uw.edu (C.D.)

Published 15 May 2020, *Sci. Adv.* **6**, eaay3188 (2020)
DOI: 10.1126/sciadv.aay3188

This PDF file includes:

Supplementary Text
Figs. S1 to S9
Table S1
References

Supplementary text

Anchovy larval abundance data treatment

Anchovy larval abundance data used in this work was sampled as part of the California Cooperative Oceanic Fisheries Investigations (CalCOFI) time series, with variable (monthly to biannual) sampling frequency from 1951 through 2011 (*23*). This timeseries was truncated to 1956-2011, as hydrographic data was not regularly collected from the SCB until 1956. Data collection occurred across large parts of the southern California Current System (CCS), and in particular within and adjacent to the Southern California Bight (SCB).

We binned larval abundance data by 1/3° latitude and longitude, and then selected a subset of the core CalCOFI sampling region (an area spanning roughly 270 km alongshore, from roughly 32°N to 34.5°N, and 270 km offshore). This area contains a geographically compact group of stations that were frequently sampled in time (greater than 100 total ship occupations within the 1/3° grid cell) while excluding a number of infrequently sampled stations farther offshore where adult or larval anchovy were rarely observed or never abundant (maximum larval abundance was generally in the hundreds dm^{-2} at stations close to shore, and <5 dm^{-2} at stations outside the area we chose).

This region is substantially similar to that used in prior analyses linking fish larval abundance to thermocline O_2 (e.g. *5, 6*), and covers the most frequent larval abundance and hydrographic observations. Other approaches have been used to assess overall anchovy stock (e.g. an area weighted approach; *12*), but in general our goal is to assess regional variability relative to habitat conditions in a defined area, rather than to assess absolute population size; more complex approaches are unnecessary for this goal. If instead we include the offshore stations (~25% of core CalCOFI stations), this choice leads to lower spatial median and mean larval abundances, and includes offshore water which has more stable seasonal and interannual dissolved oxygen (O_2) concentrations and temperature—this leads to smaller variability in calculated anomalies, but similar patterns in correlations between larval abundance and aerobic habitat across physiological traits as with the nearer to shore area used in our analysis.

For correlational analyses, larval abundance across this region was averaged over all January through April observations for each year (anchovy peak spawning season in this region; *25*, *31*). Over most of the time series, there were one or two sampling cruises in this period each year; these winter samples dominated annual abundances, and anchovy larvae tended to be more consistently observed in this season than at other times of year.

Hydrographic observations and model field data treatment

To map the spatial distribution and temporal variability of Φ in the CCS, we combined hydrographic data from historical observations and Regional Ocean Modeling System simulations. A synthesis of observational and model simulated data is used to exploit the distinct advantages of each data type. While hydrographic observations have long temporal coverage (1956–2011), the frequency of sampling in space and time is not adequate to determine aerobic habitat volumes at regional scales. Model simulated data provide more highly resolved estimates of temperature and O_2 distributions on interannual timescales from 1995–2010, but are not long enough to evaluate habitat changes over multi-decadal time-scales.

Hydrographic observations

Hydrographic data were obtained from the World Ocean Database (WOD; *46*), including CalCOFI time series data. Hydrographic data were binned by 1/3° latitude and longitude, and restricted to the same region as the anchovy larval abundance data for correlational analysis only—for mapping all available data were plotted.

While the region covered by CalCOFI is one of the most extensively sampled in the world, these data contain gaps in space and time. Therefore in order to normalize for more or less frequent sampling in different seasons throughout the year, hydrographic data were additionally seasonally binned into winter (December–February), spring (March–May), summer (June–August), and fall (September–November). These seasonal means were then averaged annually for use in the correlations, in similar manner to prior studies (*5*, *6*).

Model simulations

We use the CCS ROMS model in conjunction with the Biogeochemical Elemental Cycling model (*47*). Model simulations cover a broad CCS region from Baja California to the Alaska Gyre at 12 km resolution, and a nested grid at higher resolution (4 km) that covers the CCS over a smaller latitude range approximately spanning the coastline of the contiguous United States West Coast. The ROMS physical models use bathymetry following cell grids. Physical boundary conditions are taken from the Mercator global ocean reanalysis (GLORYS2V3; http://www.myocean.eu/) and biogeochemical boundary conditions are taken from the World Ocean Atlas climatology derived from WOD data. Additional ROMS details are found in published work using substantially similar model output (*15*-*18*). Specifically, the configuration of physical processes is similar to that described by Renault et al. 2016 (*15*), the implementation of the biogeochemistry model is similar to that in Durski et al. 2017 (*16*)—validated oxygen and temperature results in the latter are also similar to those used in the present study.

The model output of the nested 4 km resolution models used here has been extensively validated against available observational data for ocean physical and biogeochemical fields (*17*, *18*). It demonstrates a high fidelity in reproducing the mean state, variability, and trends of key tracers including temperature and O_2. The 12 km resolution ROMS output and nested ROMS 4 km model output are similar for O_2 and temperature (**Fig. S1**); the wider latitudinal range of the 12 km model is used for mapping that encompass the full anchovy range, while the 4 km nested solution is used for the statistical analysis of the larval variability in the SCB. ROMS model output was not validated for the Gulf of California, and this region is not evaluated in our analyses.

Model/data synthesis

For correlational analysis of anchovy larval abundance with aerobic habitat volume, we first calculated Φ from WOD observations, and compared these fields to Φ from the ROMS 4 km resolution output (in both cases across all ecophysiotypes). In the SCB analysis region, the volume-weighted annual mean Φ from either approach was very similar (for the ROMS hindcast years 1995–2010), and had similar interannual variability (seasonally variability could not be consistently evaluated from the observational time series). While the spatial means of Φ were very similar for any given year, in general observational data availability was too patchy (particularly with depth) to accurately estimate the total volume of aerobic habitat and its seasonal evolution.

In order to substitute model outputs for observational data, we corrected the ROMS output for the small annual mean bias between the two resulting Φ fields (-0.1 Φ). We then calculated the cumulative SCB aerobic habitat volume change (in the model) that resulted from applying the mean WOD Φ anomaly for each time series year (from the entire SCB) to each model cell in the ROMS hindcast, because the available data supports the first-order assumption that increases and decreases in the Metabolic Index were regionally coherent and approximately constant with respect to depth over the upper 100 m. In other words, the spatially averaged Φ anomalies based on the observed hydrographic time series was translated to an equivalent time series of regionally integrated habitat volume based on the explicitly calculated Φ (or,

simultaneously, Φ/Φ_{crit}) throughout the entire model domain, regardless of observational sampling gaps.

The resulting distribution of aerobic habitat with changing Φ/Φ_{crit} for any given ecophysiotype over the time series (**Fig. S9**) spans a different range of regional mean Φ relative to the critical value, and encompasses a relative habitat volume between 0 (no available habitat in a given year) and 1 (the entire 0–100 m depth is above the critical threshold and is aerobically available habitat). Over an arbitrarily large range in Φ/Φ_{crit} (greater than that seen in the time series), the habitat volume for any particular ecophysiotype would have an S-shaped response, with small or zero changes in aerobic habitat volume at very low and very high Φ (when almost all habitat is either unavailable or accessible, respectively), and large, approximately linear changes at intermediate vales where Φ is near Φ_{crit} (Φ/Φ_{crit} is near 1).

Dynamic downscaling of climate projections for 2100

Temperature and O_2 fields for 2100 were calculated using output from the following Coupled Model Intercomparison Project Phase 5 (CMIP5) Representative Concentration Pathway 8.5 models (*48*):

1. NOAA Geophysical Fluid Dynamics Laboratory, GFDL-ESM2M
2. Met Office Hadley Centre and Instituto Nacional de Pesquisas Espaciais, HadGEM2-ES
3. Institut Pierre-Simon Laplace, IPSL-CM5A-LR
4. Max-Planck-Institut für Meteorologie, MPI-ESM-LR
5. National Science Foundation - Department of Energy - National Center for Atmospheric Research, CESM1(BGC)

2071–2100 - 1971–2000 trends were obtained from each model and from the ensemble mean of the earth system models, and applied as boundary conditions to the ROMS model. Pairing climate model and ROMS hydrographic output along isopycnals is expected to improve hindcast accuracy of biogeochemical variables by limiting errors associated with shifting isopycnal depths; however, the earth system model anomalies were calculated at specified depths, and the depth of isopycnal surfaces changes in the future simulations under climate forcing, making such depth to density conversions of output impractical. Thus for this portion of the analysis depth based boundary conditions were also used for the ROMS hindcast output.

These 100-year anomalies were added to the 1995–2010 ROMS 12 km resolution hindcast boundary conditions in order to generate dynamically downscaled fields of future temperature, O_2, Φ, and alongshore aerobic habitat volumes in ROMS (other downscaled physical and biogeochemical variables will be evaluated in future work). Changes in temperature and O_2 (and thus Φ) in the upper ocean were consistent and similar across the evaluated earth system model forcings. At 100 m depth and averaged from 0-200 km offshore, the 2100 – 2000 change in O_2 was -25 to -11 mmol O_2 m^{-3} (a 9-13% decrease, 95% confidence interval), which was a significant decrease (p=0.03 for a paired t-test across models). Temperature over the same range changed by 2.0-2.3 °C (a 21-25% increase, 95% confidence interval), which was also significant across models (p=0.0008). Given the consistency across models, we chose to present ROMS forecasts from the ensemble mean temperature and O_2 of downscaled climate forcings. Compared to interpolated CMIP5 output, this ensemble downscaling leads to slightly larger decreases in O_2 in the upper 100 m of the coastal CCS, particularly to the north (**Fig. S8**, and thus slightly larger decreases in Φ and habitat volume for a given physiological hypoxia tolerance (A_o).

Physiological trait constraints from anchovy distribution

We used the time-mean distribution of anchovy to estimate their plausible combinations of Metabolic Index traits. To do this, we first had to subset the anchovy observations that could be accurately paired with hydrographic data. Anchovy observations were obtained from both the

Ocean Biogeographic Information System (OBIS; *21*) and from the National Oceanic and Atmospheric Administration (NOAA) West Coast groundfish bottom trawl survey (*22*). The OBIS samples were primarily from NOAA mid-water trawl surveys and from Department of Fisheries and Oceans Canada bottom trawls targeting shrimp. While we explicitly removed egg observations because passive drifting means that non-viable eggs can be found outside of anchovy habitat, larvae could not be clearly distinguished from juvenile and adult samples because more than half of the OBIS observations did not have life stage noted: we assumed that these were primarily juveniles and adults, given that the observations were predominantly collected via net trawls. As larvae are found near the surface (and thus in oxygen conditions set by the atmosphere) and larvae are generally found in the same regions as adults, leaving larvae in the observations is not expected to bias the results relative to an adult only distribution.

We were forced to exclude nearly half the total observations because they could not be accurately paired with either hydrographic observations or model output, leaving 1075 observations for this analysis. The excluded data generally fell into four categories: Observations from estuarine environments such as San Francisco Bay and Puget Sound, those without the month of sampling recorded (everything from the Baja Peninsula), samples with poorly constrained depths (>30 m bin or uncertainty in reported depth; missing depths were instead assumed to represent near-surface samples), and observations from depths with strong seasonal and interannual isopycnal variation, which prevented accurate pairing with hydrographic data. The latter category included all bottom trawl data, which was generally conducted over the outer continental shelf where bottom O_2 is highly variable and can span nearly the entire range between atmospheric equilibrium and anoxia.

In addition to large uncertainties related to the difference between in situ and climatological conditions at these depths, many of the bottom trawl data were additionally suspect because they included depths hundreds of meters below the observed range of anchovy based on mid-water trawls or acoustic data. It is possible that bottom depth variability over the trawls, altered anchovy behavior near a shelf-bottom trawl (e.g. avoidance and attraction), and inadvertent capture during net retrieval could have contributed to biases in reported observation depths relative to typical anchovy depth range. However, some of these observations may be accurate and could represent a temporary (e.g. daytime) deep refuge for anchovy in a resting, low activity metabolic state.

As described in the main text, the subset of 1075 observations used in the analysis were paired by month, latitude, and longitude with the nearest ROMS 4km resolution model cell. The density coordinate of each observation was determined from WOD climatological fields interpolated to the ROMS model grid, and the climatological temperature and O_2 outputs from the model for the same density was assigned to each observation for the three months surrounding sampling in order to incorporate the variable range of conditions likely to encompass the true in situ conditions associated with a particular anchovy observation. Alternatively using hydrographic data from only the months of sampling (1 month per observation) led to a more fragmented temperature-O_2 habitat space with lower *F1*-scores (unless larger variable bins were chosen), but nonetheless resulted in the same best fit ecophysiological traits.

The resulting distribution of observations in O_2-temperature space was not well described by single-variable thresholds for temperature or O_2. Instead, the boundary in O_2-temperature space between waters with and without reported anchovy occurrences is generally well-described by a curve of critical pO_2 that varies with temperature. This hypoxic threshold can be predicted from Metabolic Index ecophysiotypes; the pO_2 intercept at some reference temperature is equal to the inverse of the ecological hypoxia tolerance (A_o/Φ_{crit}) and the temperature sensitivity (E_o)

describes the changing slope of this curve with temperature. In other words, $\Phi/\Phi_{crit}=1$ at the threshold pO_2 at any given temperature, with aerobically suitable habitat at higher pO_2.

In order to distinguish between more and less likely ecophysiotypes using the occupancy boundaries from the binned hydrographic data, we evaluated the *F1*-score based on the presence and absence of anchovy in O_2-temperature bins above and below the critical pO_2. The *F1*-score is calculated as the harmonic mean of precision and recall, with equal weighting given to both measures. In this case, precision can be thought of as the probability that the presence of anchovy in O_2-temperature space is a true positive (TP; anchovy found in the space where they are predicted to occur) rather than a false positive (FP; anchovy found in a space predicted to be below the hypoxic threshold), while recall can be thought of as the probability that anchovy are actually found where they are expected to be present in that O_2-temperature space (i.e. how likely is a TP relative to a false negative, FN, missing observations above the hypoxic threshold) (*49*). In terms of these variables, the *F1*-score can be expressed as:

$$F_1 = \left(\frac{\text{recall}^{-1}+\text{precision}^{-1}}{2}\right)^{-1} = \frac{2\text{TP}}{2\text{TP}+\text{FN}+\text{FP}} \qquad \text{(S1)}$$

Thus, this metric does not give weight to absence data (true negatives) which are infrequently and inconsistently reported in fisheries data, but allows us to optimize between ecophysiotypes that constrain too small an O_2-temperature space but maximize presence within that space (high recall but low precision) and ecophysiotypes that hardly constrain habitat but contain all observations (high precision but low recall). A model with perfect precision and recall would have *F1*=1. However, environmental observations are by nature patchy in space and time, meaning false negatives are unavoidable (anchovy are not observed where there was no sampling), and climatological hydrographic data does not perfectly match in situ conditions, meaning false positives are likely (anchovy are present at a location when conditions were more favorable than the climatological hydrographic conditions in the observation space). Further, the *F1*-score depends on the range of state-space evaluated; an evaluation over a temperature range of 0-30°C would include mostly space with no presence or absence information, leading to low values. Thus *F1* rarely exceeded 0.7 for the evaluated ecophysiotypes, but regardless of the particular range of conditions evaluated the relative scores between trait combinations are conserved.

Correlational analysis of larval abundance and hydrographic data

For all combinations of potential Metabolic Index traits, we computed annual mean Φ from WOD observations, translated this to an expected aerobic habitat volume (volume in a specified southern CCS region and 0-100 m depth range with $\Phi/\Phi_{crit}>1$) from the ROMS simulations, and correlated Φ and habitat volume with spawning season anchovy larval abundance. Specifically, we used a Model II regression ("gmregress" function for Matlab; *50*), in which both aerobic habitat volume (or Φ) and larval abundance are assumed to have random errors and neither variable is assumed to be significantly more precise *a priori*. In this approach, the offsets between observed and predicted values are calculated normal to the regression line in order to minimize the misfit of variables along both axes. The residuals of the regression models for anchovy larval abundance as a function of aerobic habitat volume were normally distributed—Anderson-Darling tests reject a non-normal error distribution at the 5% significance level for all ecophysiotypes resulting in significant correlations ($p<0.05$)—and thus the squared correlation coefficient (r^2) is equivalent to the fraction of total variance shared between larval abundance and habitat volume resulting from each physiological parameter combination.

Across ecophysiotypes, resulting correlations explained between 0 and 40% of interannual variance (unsmoothed data), or up to 75% of decadal variance (where anchovy larval abundance and aerobic habitat were smoothed by a 10 year moving average to remove short period fluctuations). Ecophysiotypes with higher correlation coefficients were judged to be more

likely to represent anchovy. Regressions of the unsmoothed (interannual) data explained less variance than the decadally smoothed data because, in part, anchovy larvae reached near zero abundance during parts of the 1950s and much of the 2000s, but this threshold occurred at greater than zero Φ (and resulting habitat volume). In other words, the natural zero thresholds of the two variables are offset by the value Φ_{crit}, at some greater than zero volume of available habitat that is nonetheless associated with low larval abundance and other indicators of stock collapse (*12*). Thus habitat volume variance below this threshold must be completely decorrelated from larval abundance. Other sources of mismatch at interannual scales may include larval advection in and out of the region, particularly successful or unsuccessful larval cohorts, spatial or temporal biases in hydrographic sampling or data accuracy (e.g. the variability between analysts in O_2 accuracy via Winkler titration), and El Niño impacts on hydrography or ecosystems. Despite these many possible confounding factors, the interannual regressions are consistent with up to 40% of the changes in anchovy larval abundance resulting from changes in aerobic habitat volume.

Multi-year or decadal moving averages reduces random biases and highlights the even stronger longer period correlation between aerobic habitat and anchovy larval abundance, and the expense of smoothing over shorter term variability that may in fact be related to shorter term perturbations in habitat. For the purposes of selecting likely ecophysiotypes, we used a 5 year moving average as a reasonable compromise between retaining too much noise and over-smoothing the time series. While the choice of moving average period changed the absolute fraction of variance explained, the relative results across ecophysiotypes (higher versus lower r^2) were consistent across averaging periods (one year to one decade).

Weighted-likelihood estimates of anchovy ecophysiological traits

We inferred the most likely physiological trait range for anchovy based on both the larval time series analysis and the adult range distribution by comparing a cost function for each combination of ecological hypoxia tolerance (A_o/Φ_{crit}) and temperature sensitivity (E_o). Specifically, we determined a relative weighting for each ecophysiotype (W_e) based on the larval-habitat volume squared correlation coefficients and the *F1*-scores from the bounded O_2-temperature space. In order to assign both measures equal importance in determining likely ecophysiotypes, we added standardized anomalies of both metrics (Δ_σ=[value-mean]/[standard deviation], where the mean and standard deviation are calculated across results from all ecophysiotypes) Then W_e is calculated as:

$$W_e = \left(\Delta_{\sigma,r^2} + f\Delta_{\sigma,F_1}\right) \qquad \text{(S2)}$$

By adding standardized anomalies, higher than average r^2 and F_1-scores are weighted more strongly, while lower than average anomalies are given negative weights which reduce W_e. f is a weighting factor that allows greater or lesser weight to be assigned to the distribution derived traits than to the larval abundance time series; in our analysis we set it to 2 as we believe the distribution could be more directly linked to adult anchovy ecophysiological constraints than the larval time series. In practice this weighting makes a very small difference in the relative weighting of most ecophysiotypes (for f between 0.25 and 4), shifting the single best fit temperature sensitivity (E_o) by 0.15 eV or less, and ecological temperature sensitivity (A_o/Φ_{crit}) by 0.4 atm^{-1} or less because of the strong concordance between the two independent approaches.

In order to bound likely traits visually (**Fig. S4**), we rescale W_e between 0 and 1 and sort from highest to lowest weights (i.e. determine the cumulative relative likelihoods for each ecophysiotypes). No single ecophysiotype is dramatically more likely (higher weight) than all others, though we use the single likeliest parameter combination (E_o=0.4 eV, A_o/Φ_{crit}=5.4 atm^{-1}) for the purposes of mapping habitat in the analysis presented in the main text. A compact range of Metabolic Index traits can nonetheless be identified to account for any specified proportion of the total likelihood; in **Fig. S4**, we plot contiguous bounds around the ecophysiotypes with the

strongest weights which cumulatively account for the upper 20% of the total likelihood, and thus are expected to contain the true anchovy traits. Regardless of whether a likelihood threshold is set at 20%, 50%, or any other arbitrary value, only certain combinations of E_o and A_o/Φ_{crit} are likely (following a convex arc from bottom right to top left of **Fig. S4**)—these likely combinations lead to compensating effects between hypoxia tolerance and temperature sensitivity thus all result in a similar net response to aerobic habitat variability. Likely ecophysiotypes are bounded in a relatively small region of trait space; the entire evaluated trait space is not shown within **Fig. S4** (this contains ~1/6 of the total evaluated range from A_o/Φ_{crit}=0 to 15 atm^{-1}). Values of the ecological hypoxia sensitivity (A_o/Φ_{crit}) below about 3.8 atm^{-1} require pO_2 higher than typically found in the CCS (>0.26 atm, ~25% supersaturated with respect to atmospheric O_2). The highest likelihood traits (with $r^2 \geq 0.5$ and $F1 \geq 0.7$) span E_o=0.2 to 0.6 eV and A_o/Φ_{crit}=4.5 to 5.8 atm^{-1}, similar to the mean of other species found within the CCS.

For the purposes of determining a weighted mean response of anchovy larval abundance to changing aerobic habitat volume, we exclude the lowest weight ecophysiotypes from further analysis, those that collectively account for less than 50% of the cumulative likelihood. In other words, the ecophysiotypes with lower than the average values of both r^2 and F_1-scores show little skill at predicting anchovy response and presence and are unlikely to include the true anchovy ecophysiotype; these were evaluated solely because they fall within the global inter-specific range, not because they are plausible for a forage fish living in generally normoxic conditions. We use W_e for the remaining ecophysiotypes to regress anchovy larval abundance on the weighted-mean relative habitat volume change (Matlab “fit” function, with linear-bisquare regression for robust fitting of weighted variables). This choice makes the weighted-mean response of anchovy to habitat loss more closely aligned with the relatively few, clustered ecophysiotypes with high weights. Other weighting choices are possible, but in general this threshold approach is a simple way to focus our analysis around the ecophysiotypes most congruent with the available data, without resorting to more complicated weighting schemes to ameliorate biases to the mean response from the large range of traits with very low predictive power.

Supplementary Figures

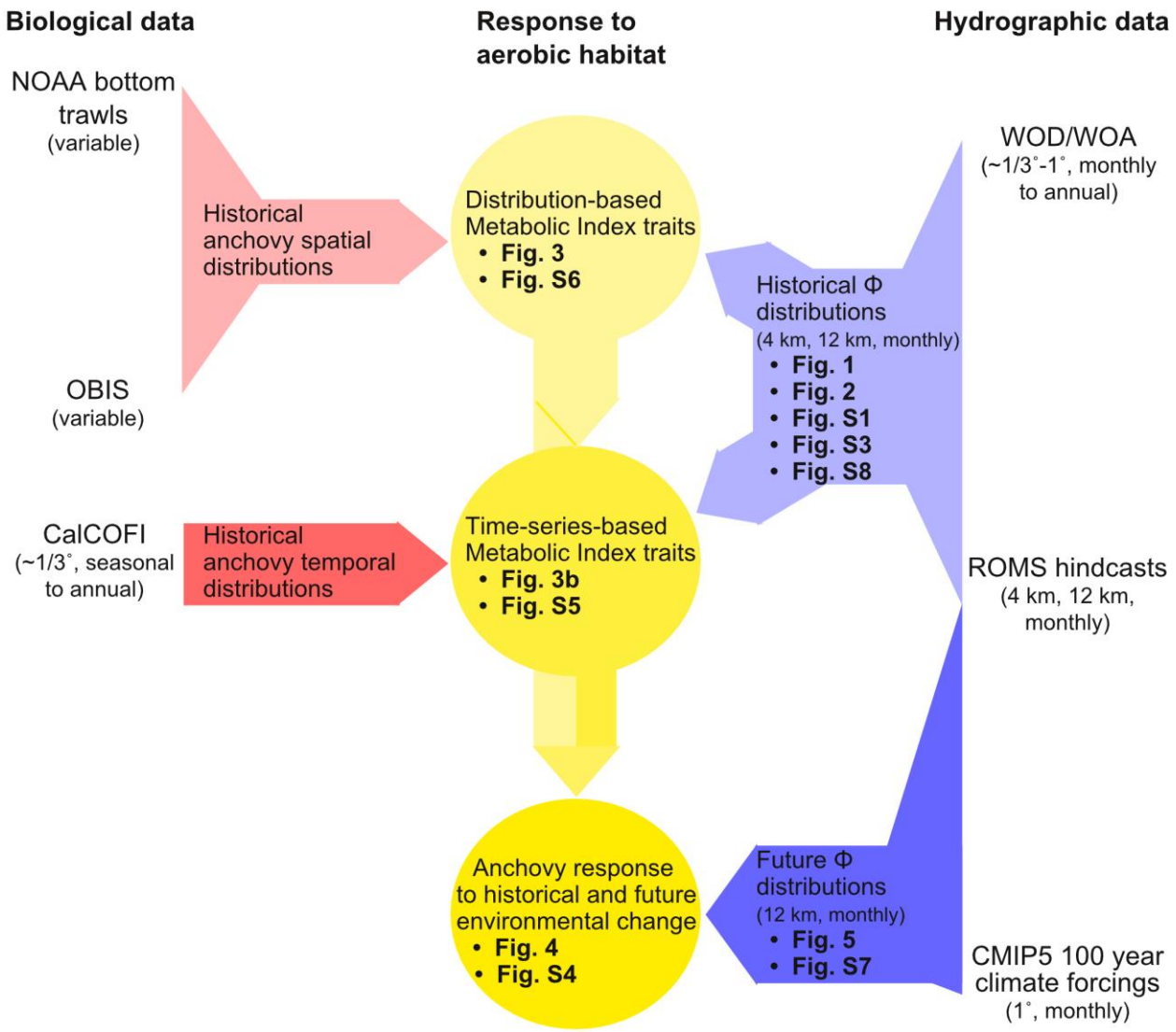

Fig. S1. Schematic diagram of analyses
Biological and hydrographic data with different limitations and complimentary coverage in spatial and temporal extent are combined in order to evaluate how the distribution of northern anchovy responds to variability in the Metabolic Index of temperature-dependent hypoxia and aerobic habitat availability. In particular, anchovy observations from the NOAA West Coast bottom trawl surveys and OBIS data have irregular temporal and spatial resolution, but wide spatial coverage, while the CalCOFI ithyoplankton dataset has high temporal resolution over several decades, but only over a small region. Hydrographic data from WOD has variable spatial and temporal coverage, with relatively high resolution in the CalCOFI but coarser temporal and spatial resolution over the broader CCS region. ROMS hydrographic simulations are available at both high spatial and temporal resolution compared to the hydrographic observations. ROMS 4 km output has higher spatial resolution that increases the precision of aerobic habitat assessment in the Southern California Bight, but has a smaller spatial extent over the CCS than the 12 km output. CMIP5 climate projections have coarse spatial and temporal resolution, but resulting forcings can be dynamically downscaled through the higher resolution ROMS model. Northern anchovy Metabolic Index traits derived from spatial distributions can be used to predict temporal responses to environmental change, which can be tested or independently evaluated using temporal biological and hydrographic data.

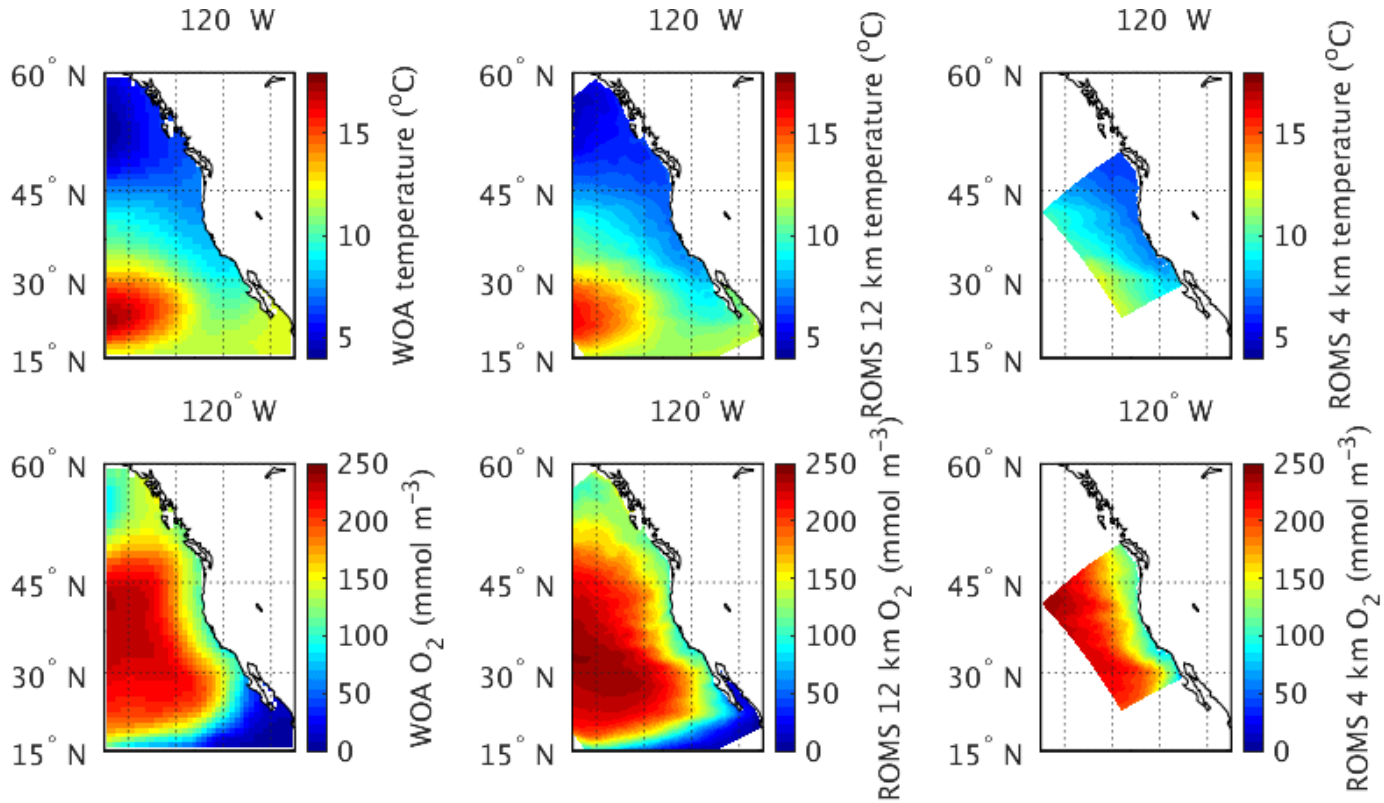

Fig. S2. Comparison of hydrographic data and ROMS models
Climatological annual mean temperature and O_2 fields at 200 m depth from the climatological World Ocean Atlas (derived from the World Ocean Database; 1955-2013), ROMS 12 km resolution hindcast model (1995-2010), and ROMS 4 km resolution hindcast model (1995-2010). Physical and biogeochemical output from the 4 km resolution hindcast has been extensively validated (*17*, *18*).

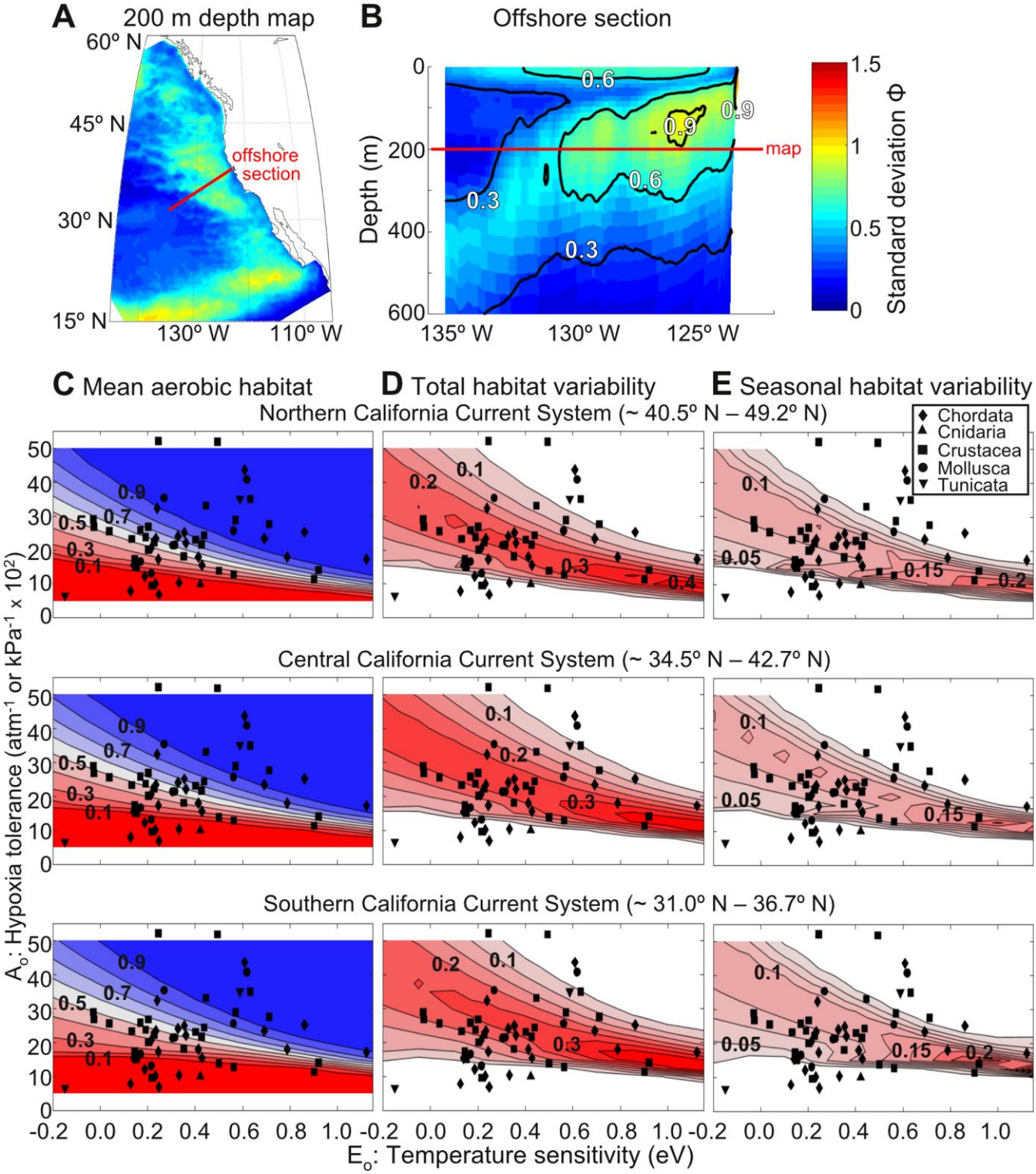

Fig. S3. Variability of the Metabolic Index (Φ) and aerobic habitat in the CCS
(**A**) Standard deviation of Φ (with hypoxia tolerance A_o=25 atm^{-1}, temperature sensitivity E_o=0.4 eV) for 12 km resolution ROMS output at 200 m depth. Red line marks offshore depth section (**B**) from 4 km resolution model (red line on section indicates depth of map plot). Mean Φ roughly 2.5–5.5 at 200 m depth, increasing offshore (**Fig. 1** in main text); i.e. relative standard deviation decreases from ~25% at shore to <5% at subtropical gyre end of section. Across physiological traits (hypoxia tolerance, A_o, temperature sensitivity, E_o), (**C**) the spatial average of mean aerobically suitable habitat volume in time, assuming ratio of active to resting metabolic

rates Φ_{crit}=3.5, expressed as a fraction of total volume in the northern, southern, and central California Current System from 4 km resolution ROMS output (0–200 km offshore, and 0–200 m depth). Approximate latitudinal range at shore noted above each row (some overlap because model grid is not aligned with latitude). (**D**) Spatial average of total variability (as standard deviation) of this habitat volume in time. (**E**) Spatial average of seasonal variability with time. Physiological traits from global species compilation marked with filled black symbols for specific (sub)phyla (♦ Chordata, ▲ Cnidaria, ■ Crustacea, ● Mollusca, and ▼ Tunicata).

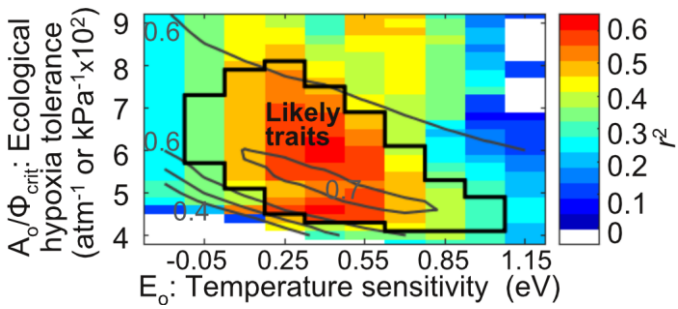

Fig. S4. Likely anchovy traits based on distribution and time-series approaches
Squared correlation coefficients (r^2) of correlations between standardized anomalies of larval abundance and habitat volume, across ecophysiological traits. *F1*-score (grey contours), inferred from fit to climatological O_2-temperature space bounding anchovy observations. Likely traits (black contour; top 20% of cumulative weight across ecophysiotypes) for anchovy based on weighted-mean combination of both approaches.

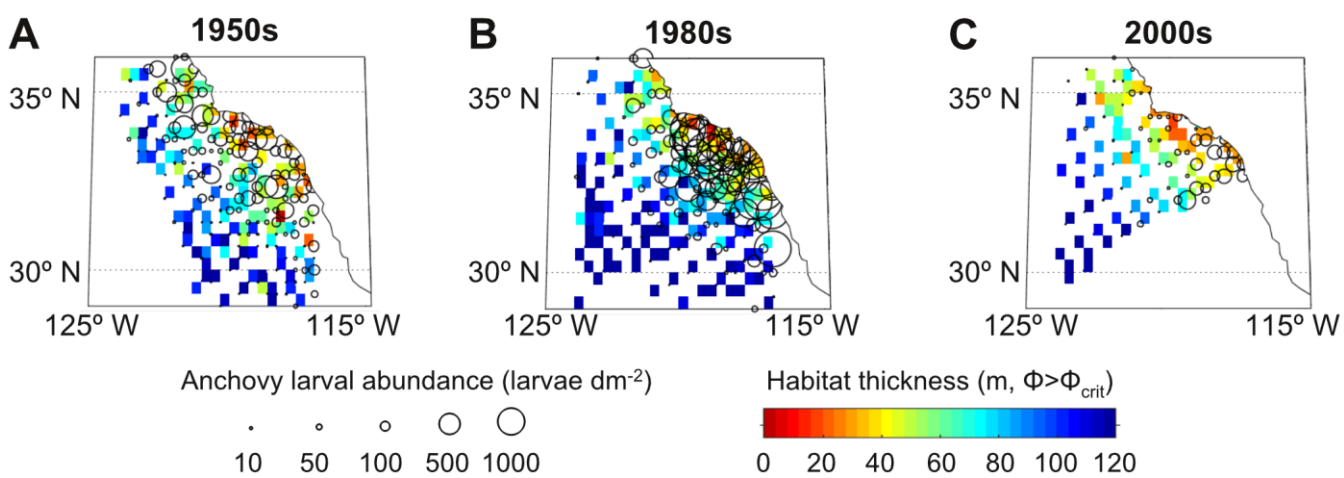

Fig. S5. Decadal changes in anchovy larval abundance and aerobic habitat
Mean abundance of anchovy larvae (black circles) and aerobic habitat thickness, the depth of water column with $\Phi \geq \Phi_{crit}$ (for A_o/Φ_{crit}=5.4 atm^{-1}, E_o=0.4 eV) from available CalCOFI and WOD hydrographic data (larval and hydrographic data in 1/3° bins). Larval abundance is calculated over January through April (peak anchovy spawning season in Southern California bight), and habitat thickness is based on decadal averages of seasonally binned aerobic habitat (all seasons) derived from hydrographic observations. Anchovy larval abundance in the Southern California Bight is (**A**) low in the 1950s, (**B**) greatest in the 1980s, and (**C**) lowest in the 2000s, similar to regional scale decreases in regional aerobic habitat thickness. Regions of

climatologically low or high habitat thickness vary seasonally, and narrow aerobic habitat in these plots reflects the influence of seasonal upwelling.

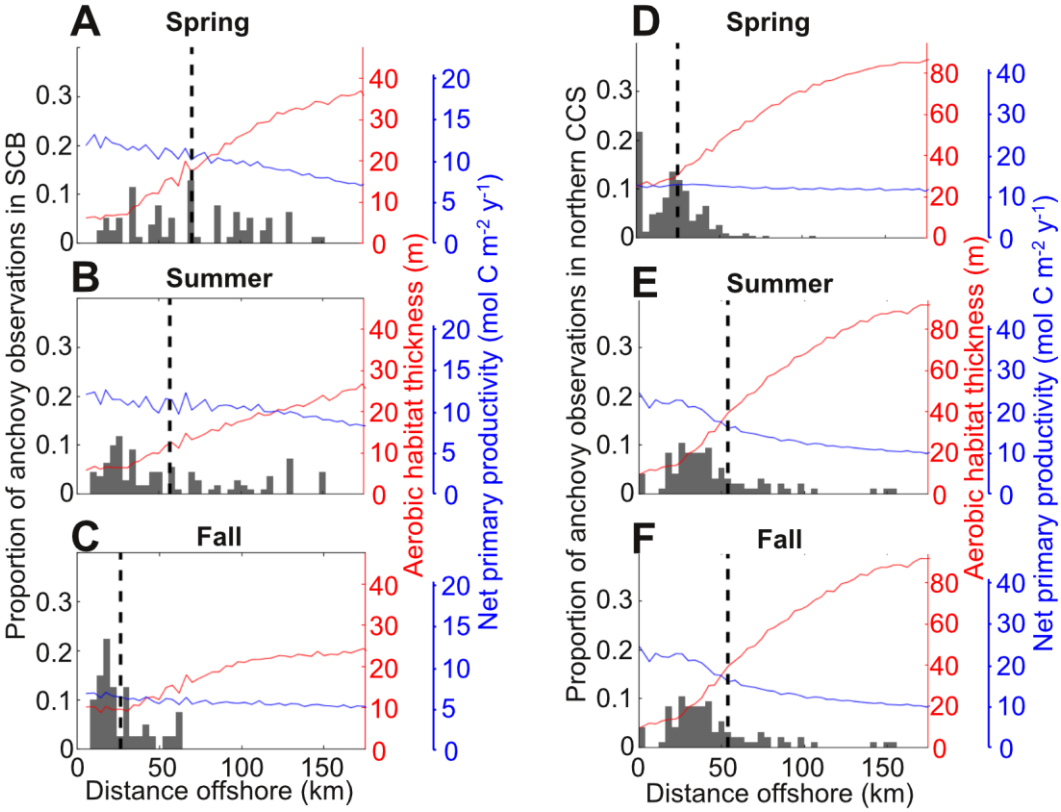

Fig. S6. Seasonal offshore distributions of anchovy, aerobic habitat, and productivity Cross-shore distributions of anchovy observations, and aerobic habitat thickness (A_o/Φ_{crit}=5.4 atm^{-1}, E_o=0.4 eV) and net primary productivity from ROMS 12 km output in the SCB" (**A**) Spring, peak upwelling season, (**B**) summer, with weakening upwelling, and (**C**) fall, with little upwelling. The same variables in the northern CCS (44°N to 50°N plotted here), in (**D**) spring, with little upwelling, (**E**) summer, peak upwelling season, and (**F**) fall, with weakening upwelling. Note larger scale for habitat thickness and net primary productivity for northern CCS. The mean location of observations dashed black lines) shifts offshore during upwelling.

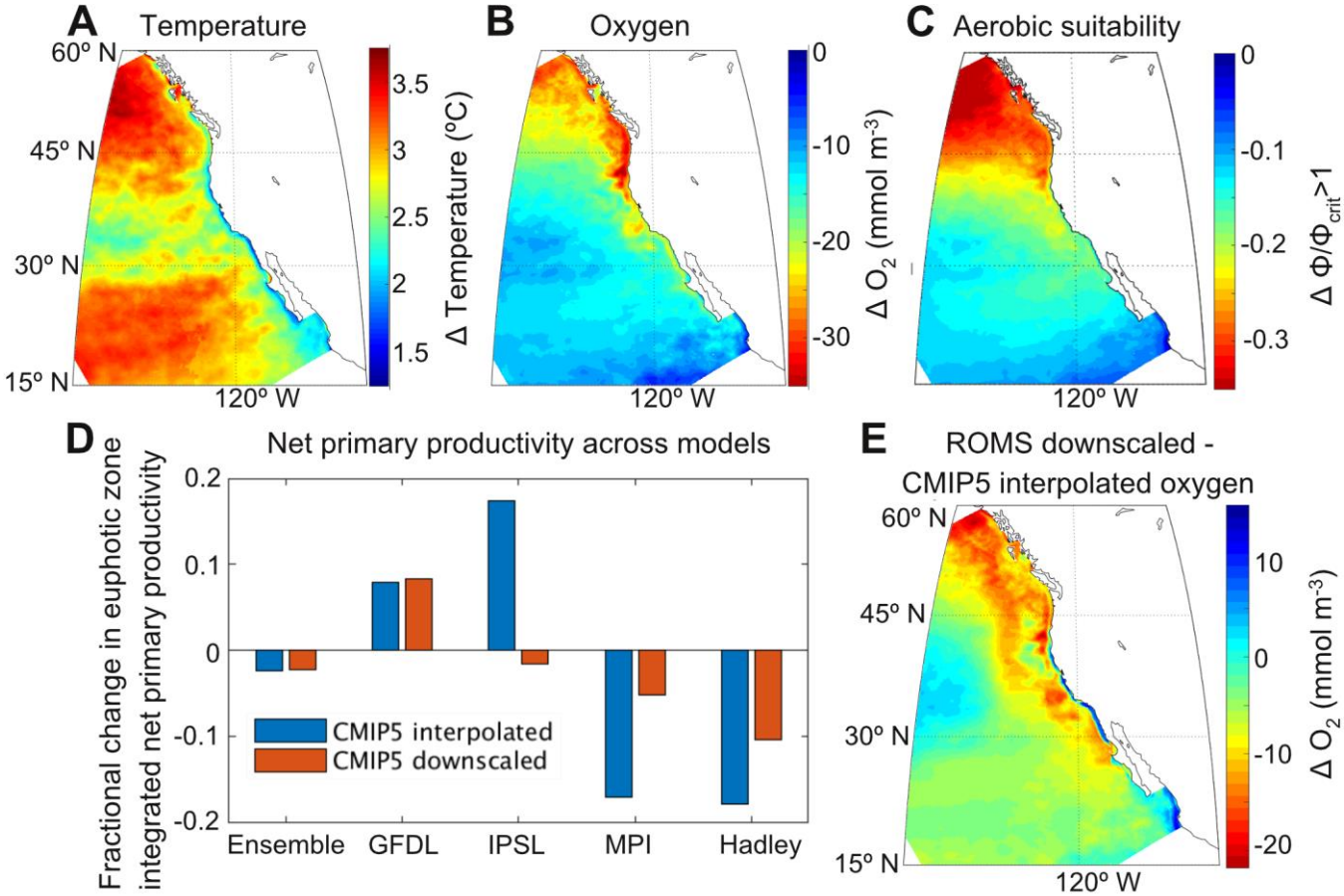

Fig. S7. 2100 - 2000 change in hydrographic conditions

2100 - 2000, 0 – 100 m annual difference (Δ) of (**A**) temperature, (**B**) oxygen (O_2), and (**C**) fraction of upper 100 m that is aerobically suitable ($\Phi/\Phi_{crit}>1$) for ecophysiological traits $A_o/\Phi_{crit}=5.4$ and $E_o=0.4$ eV. Differences generated from ROMS 12 km resolution hindcast with and without 100 year hydrographic anomalies (2071–2100 - 1971–2000) from downscaled CMIP5 models. Ensemble mean of results of individual CMIP5 model downscalings presented. (**D**) In contrast to temperature and O_2, the 2100 - 2000 relative change of annual mean euphotic zone integrated net primary production does not agree in direction or magnitude across global scale earth system models interpolated to the ROMS grid, or ROMS forecasts with dynamically downscaled forcings (here integrated from 0-200 km offshore in the CCS and normalized to the ROMS 12 km hindcast mean). This plot excludes NCAR model output which did not include wind fields needed to simulate changes in vertical transport in the same manner as the other models. The ensemble mean changes are small in either the interpolated or downscaled cases (<3%).

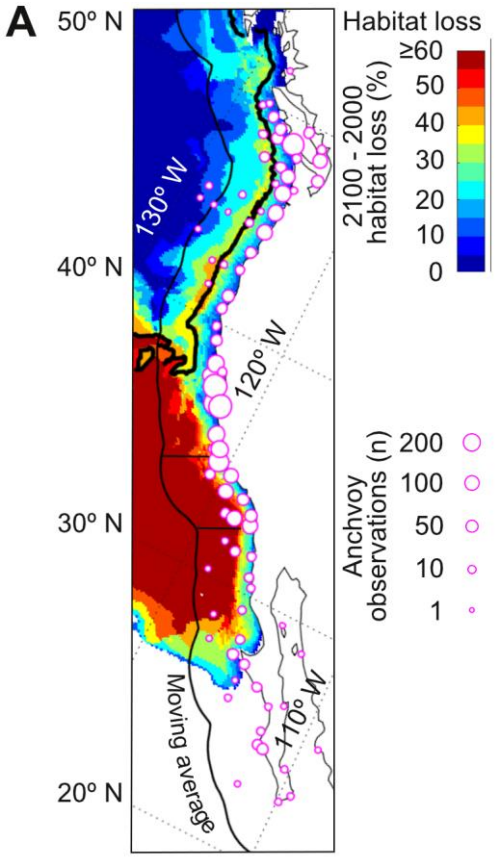

Fig. S8. Aerobic habitat compression for anchovy

Aerobic habitat compression, 2100 - 2000 (12 km resolution ROMS with RCP 8.5 climate forcings), overlaid with anchovy observations (circles) and aerobic habitat threshold value associated with historically low larval abundance (2100, thick black line). This threshold value is only meaningful when integrated over a similarly sized region to the SCB, from which it was derived. Thus both this threshold and the extent of non-zero aerobic habitat are translated into range limits via moving average habitat integration (along thin black lines) in order to determine annual average range limits.

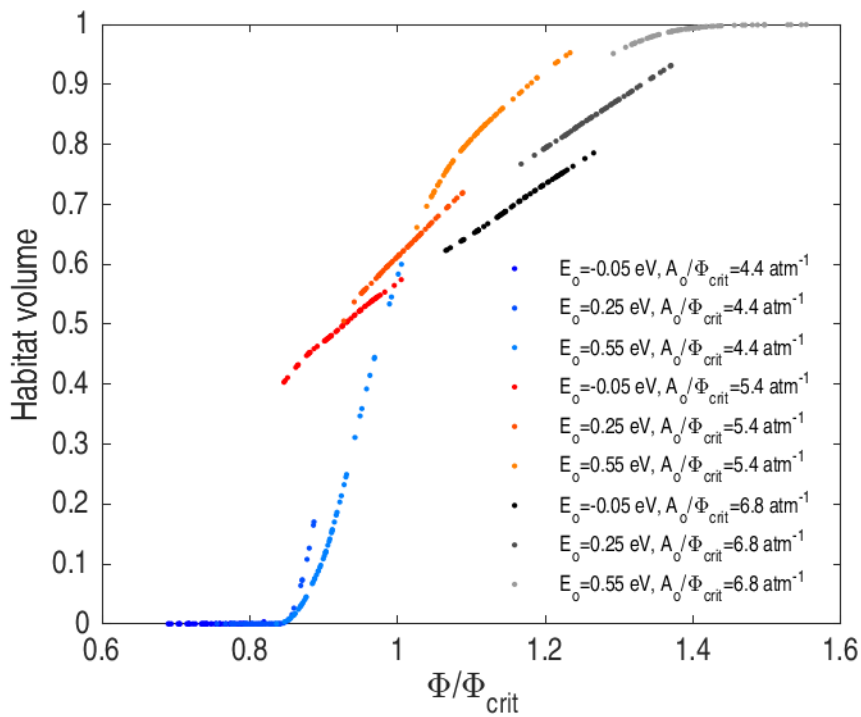

Fig. S9. Relationships between habitat volume and Metabolic Index (Φ)
Example solutions of relative habitat volume (0 to 1, where 1 indicates entire upper 100 m is aerobically suitable habitat) over the hydrographic time series, as a function of ROMS volume averaged Φ/Φ_{crit} for a given ecophysiotype and anomaly in mean Φ/Φ_{crit} from the hydrographic observations. Time series are plotted for ecophysiotypes including three values of temperature sensitivity (E_o) and three values of the ecological hypoxia tolerance (A_o/Φ_{crit}), spanning low to moderate hypoxia tolerances and low to moderate temperature sensitivities (at high values of both all habitat volume is aerobically suitable). Volume averaged Φ/Φ_{crit} entirely higher or lower than 1 over the time series does not preclude a subset of the overall environment from being below or above the threshold. Habitat volume changes are normalized to the mean for each ecophysiotype when evaluating the weighted average response across ecophysiotypes.

Table S1. Ecophysiological traits for California Current system species

Metabolic Index ecophysiological traits for species found in the California Current System (CCS; *9*), including hypoxia tolerance (A_o), the temperature dependence of that hypoxia tolerance (E_o), and the active to resting metabolic ratio (Φ_{crit}) inferred from biogeographic species distributions. Increasing A_o or decreasing Φ_{crit} have equivalent effects on the threshold value of $\Phi/\Phi_{crit} \geq 1$ for aerobically suitable habitat, thus A_o/Φ_{crit} normalizes the net effects of both physiological and ecological hypoxia tolerance on aerobic habitat for inter-species comparisons.

Species	Common name	Vertical range*	A_o (atm^{-1})	E_o (eV)	Φ_{crit}	A_o/Φ_{crit} (atm^{-1})
		Native to CCS				
Acanthephyra curtirostris	peaked shrimp	meso-, bathypelagic	25.6	0.04		
Bythograea thermydron	hydrothermal vent crab	benthic (>2000 m)	52.8	0.23		
Desmophyllum pertusa	deep water coral	benthic (>100 m)	9.9	0.44	1.4	7.1
Dosidicus gigas	Humboldt squid	mesopelagic	40.8	0.62		
Engraulis mordax[b]	northern anchovy	epipelagic		0.4 (0.1–0.7) †		5.4 (4.4–6.6) †
Penaeus vannamei	whiteleg shrimp	benthic (<100 m)	59.4	0.09		
Melanostigma pammelas	midwater eelpout	mesopelagic	19.1	1.06		
Pandalus platyceros	California spot prawn	benthic (<3000 m)	18.9	0.15	1.8	10.5
Panulirus interruptus	California spiny lobster	benthic (<200 m)	28.9	0.57		
Stenobrachius leucopsarus	Northern lampfish	epi-, mesopelagic	23.4	0.69	2.2	10.6
Tarletonbeania crenularis	blue lanternfish	epi-, mesopelagic	20.6	0.21	2.6	7.9
		Invasive or introduced to CCS				
Carcinus maenas	European green crab	benthic (<100 m)	22.3	0.48		
Salmo salar	Atlantic salmon	epipelagic	10.4	0.34		
Styela plicata	pleated sea squirt	benthic (<100 m)	6.3	-0.09	1.4	4.5
Morone saxatilis	striped bass	epipelagic	24.0	0.33	5	4.8

* Vertical range for pelagic organisms qualitatively binned by epipelagic (0–200 m), mesopelagic (200–1000 m), or bathypelagic (1000–4000 m) based on preponderance (>80%) of observations in data with depth information in OBIS. Upper or lower range limits for benthic organisms estimated to nearest 100 m (1000 m or less) or 1000 m (greater than 1000 m) based on preponderance (>80%) of OBIS data with depth information.

† Traits inferred in this work, presented as single most likely weighted trait pair from analysis using both larval abundance time series and adult time-mean distribution, and (in parentheses) the range of values encompassing >10% cumulative likelihood of trait values over the entire evaluated range of traits (i.e. a compact subset of most likely ecophysiotypes); alternatively traits with >20% of cumulative likelihood across evaluated ecophysiotypes are shown in **Fig. S4**.

REFERENCES AND NOTES

1. IPCC, *Climate Change 2014: Impacts, Adaptation, and Vulnerability. Part A: Global and Sectoral Aspects. Contribution of Working Group II to the Fifth Assessment Report of the IPCC* (Cambridge Univ. Press, 2014), 1132 pp.

2. M. C. Long, C. Deutsch, T. Ito, Finding forced trends in oceanic oxygen. *Global Biogeochem. Cycles* **30**, 381–397 (2016).

3. Northwest Fisheries Science Center, Ecosystem status report of the California Current for 2017: A summary of ecosystem indicators compiled by the California Current Integrated Ecosystem Assessment Team (CCIEA) (NOAA Technical Memorandum NMFS-NWFSC, NOAA, 2017).

4. E. Di Lorenzo, V. Combes, J. E. Keister, P. T. Strub, A. C. Thomas, P. J. S. Franks, M. D. Ohman, J. C. Furtado, A. Bracco, S. J. Bograd, W. T. Peterson, F. B. Schwing, S. Chiba, B. Taguchi, S. Hormazabal, C. Parada, Synthesis of Pacific Ocean climate and ecosystem dynamics. *Oceanography* **26**, 68–81 (2013).

5. J. A. Koslow, R. Goericke, A. Lara-Lopez, W. Watson, Impact of declining intermediate-water oxygen on deepwater fishes in the California Current. *Mar. Ecol. Prog. Ser.* **436**, 207–218 (2011).

6. J. A. Koslow, R. Goericke, W. Watson, Fish assemblages in the Southern California Current: Relationships with climate, 1951-2008. *Fish. Oceanogr.* **22**, 207–219 (2013).

7. A. A. Keller, L. Ciannelli, W.W. Wakefield, V. Simon, J.A. Barth, S.D. Pierce, Species-specific responses of demersal fishes to near-bottom oxygen levels within the California Current large marine ecosystem. *Mar. Ecol. Prog. Ser.* **568**, 151–173 (2017).

8. C. Deutsch, A. Ferrel, B. Seibel, H.-O. Pörtner, R. B. Huey, Climate change tightens a metabolic constraint on marine habitats. *Science* **348**, 1132–1135 (2015).

9. J. L. Penn, C. Deutsch, J. L. Payne, E. A. Sperling, Temperature-dependent hypoxia explains biogeography and severity of end-Permian marine mass extinction. *Science* **362**, eaat1327 (2018).

10. H.-O. Pörtner, R. Knust, Climate change affects marine fishes through the oxygen limitation of thermal tolerance. *Science* **315**, 95–97 (2007).

11. C. C. Peterson, K. A. Nagy, J. Diamond, Sustained metabolic scope. *Proc. Natl. Acad. Sci. U.S.A.* **87**, 2324–2328 (1990).

12. A. D. MacCall, W. J. Sydeman, P. C. Davison, J. A. Thayer, Recent collapse of northern anchovy biomass off California. *Fish. Res.* **175**, 87–94 (2016).

13. A. Bertrand, A. Chaigneau, S. Peraltilla, J. Ledesma, M. Graco, F. Monetti, F. P. Chavez, Oxygen: A fundamental property regulating pelagic ecosystem structure in the coastal Southeastern Tropical Pacific. *PLOS ONE* **6**, e29558 (2011).

14. A. L. Perry, P. J. Low, J. R. Ellis, J. D. Reynolds, Climate change and distribution shifts in marine fishes. *Science* **308**, 1912–1915 (2005).

15. L. Renault, C. Deutsch, J. C. McWilliams, H. Frenzel, J.-H. Liang, F. Colas, Partial decoupling of primary productivity from upwelling in the California Current system. *Nat. Geosci.* **9**, 505–508 (2016).

16. S. M. Durski, J. A. Barth, J. C. McWilliams, H. Frenzel, C. Deutsch, The influence of variable slope-water characteristics on dissolved oxygen levels in the northern California Current System JGR. *Oceans* **122**, 7674–7697 (2017).

17. C. Deutsch, H. Frenzel, James C. Mc Williams, L. Renault, F. Kessouri, E. Howard, J.-H. Liang, D. Bianchi, S. Yang, Biogeochemical variability in the California Current System. bioRxiv 942565 [**Preprint**]. 11 February 2020. https://doi.org/10.1101/2020.02.10.942565.

18. L. Renault, J. C. McWilliams, A. Jousse, C. Deutsch, H. Frenzel, F. Kessouri, The physical structure and behavior of the california current system. bioRxiv 942730 [**Preprint**]. 12 February 2020. https://doi.org/10.1101/2020.02.10.942730.

19. R. A. Meyers, When do environment-recruitment correlations work? *Rev. Fish Biol. Fisheries* **8**, 285–305 (1998).

20. C. M. Beale, J. J. Lennon, A. Gimona, Opening the climate envelope reveals no macroscale associations with climate in European birds. *Proc. Natl. Acad. Sci. U.S.A.* **105**, 14908–14912 (2008).

21. OBIS and data contributors, Distribution records of *Engraulis mordax* (Girard 1854), and other species, 1953–2015. OBIS data server (2019); http://iobis.org/.

22. National Oceanic and Atmospheric Administration Northwest Fishery Science Center, Trawling records of *Engraulis mordax* from West Coast groundfish bottom trawl surveys. NWFSC Fishery Resource Analysis and Monitoring Data Warehouse (2019); https://www.nwfsc.noaa.gov/data/.

23. CalCOFI and data contributors, CalCOFI icthyoplankton database, 1951–2011. NOAA ERDDAP data server (2016); https://coastwatch.pfeg.noaa.gov/erddap.

24. J. A. Koslow, P. Davison, A. Lara-Lopez, M. D. Ohman, Epipelagic and mesopelagic fishes in the southern California Current System: Ecological interactions and oceanographic influences on their abundance. *J. Mar. Syst.* **138**, 20–28 (2014).

25. K. F. Mais, Pelagic fish surveys in the California Current. *Cal. Fish Game Fish. Bull.* **162**, 1–79 (1974).

26. J. L. Laroche, S. L. Richardson, Reproduction of northern anchovy, *Engraulis mordax*, off Oregon and Washington. *NOAA Fish. Bull.* **78**, 603–618 (1980).

27. E. Di Lorenzo, Seasonal dynamics of the surface circulation in the Southern California Current System. *Deep Sea Res. Part II Top Stud. Oceanogr.* **50**, 2371–2388 (2003).

28. D. R. Munro, P. D. Quay, L. W. Juranek, R. Goericke, Biological production rates off the Southern California coast estimated from triple O_2 isotopes and O_2: Ar gas ratios. *Limnol. Oceanogr.* **58**, 1312–1328 (2013).

29. C. W. Haugen, J. D. Messersmith, R. H. Wickwire, Progress report on anchovy tagging off California and Baja California, March 1966 through May 1969. *Cal. Fish Game Fish. Bull.* **147**, 75–89 (1969).

30. J. Fiechter, K. A. Rose, E. N. Curchitser, K. S. Hedstrom, The role of environmental controls in determining sardine and anchovy population cycles in the California Current: Analysis of an end-to-end model. *Prog. Oceanogr.* **138**, 381–398 (2015).

31. R. D. Methot, Synthetic estimates of historical abundance and mortality for northern anchovy. *Am. Fish. Soc. Sym.* **6**, 66–82 (1989).

32. M. G. Hammann, M. A. Cisneros-Mata, Range extension and commercial capture of the northern anchovy, *Engraulis mordax* Girard, in the Gulf of California, Mexico. *Cal Fish Game* **75**, 49–53 (1989).

33. F. P. Chavez, J. Ryan, S. E. Lluch-Cota, M. Ñiquen, From anchovies to sardines and back: Multidecadal change in the Pacific Ocean. *Science* **299**, 217–221 (2003).

34. M. Lindegren, D. M. Checkley Jr., T. Rouyer, A. D. MacCall, N. C. Stenseth, Climate, fishing, and fluctuations of sardine and anchovy in the California Current. *Proc. Natl. Acad. Sci. U.S.A.* **110**, 13672–13677 (2013).

35. C. Deutsch, H. Brix, T. Ito, H. Frenzel, L. Thompson, Climate-forced variability of ocean hypoxia. *Science* **333**, 336–339 (2011).

36. D. M. Checkley Jr., R. G. Asch, R. R. Rykaczewski, Climate, anchovy, and sardine. *Ann. Rev. Mar. Sci.* **9**, 469–493 (2017).

37. K. L. Robinson, J. J. Ruzicka, M. B. Decker, R. D. Brodeur, F. J. Hernandez, J. Quiñones, E. M. Acha, S.-i. Uye, H. Mianzan, W. M. Graham, Jellyfish, forage fish, and the world's major fisheries. *Oceanography* **27**, 104–115 (2014).

38. C.-H. Hsieh, C. Reiss, W. Watson, M. J. Allen, J. R. Hunter, R. N. Lea, R. H. Rosenblatt, P. E. Smith, G. Sugihara, A comparison of long-term trends and variability in populations of larvae of exploited and unexploited fishes in the Southern California region: A community approach. *Prog. Oceanogr.* **67**, 160–185 (2005).

39. J. S. Stewart, E. L. Hazen, S. J. Bograd, J. E. K. Byrnes, D. G. Foley, W. F. Gilly, B. H. Robison, J. C. Field, Combined climate- and prey-mediated range expansion of Humboldt squid (*Dosidicus gigas*), a large marine predator in the California Current System. *Glob. Chang. Biol.* **20**, 1832–1843 (2014).

40. B. A. Seibel, N. S. Hafker, K. Trubenbach, J. Zhang, S. N. Tessier, H. O. Pörtner, R. Rosa, K. B. Storey, Metabolic suppression during protracted exposure to hypoxia in the jumbo squid, Dosidicus gigas, living in an oxygen minimum zone. *J. Exp. Biol.* **217**, 2555–2568 (2014).

41. R. Salvatteci, D. Field, D. Gutiérrez, T. Baumgartner, V. Ferreira, L. Ortlieb, A. Sifeddine, D. Grados, A. Bertrand, Multifarious anchovy and sardine regimes in the Humboldt Current System during the last 150 years. *Glob. Chang. Biol.* **24**, 1055–1068 (2018).

42. F. LeComte, W. S. Grant, J. J. Dodson, R. Rodriguez-Sanchez, B. W. Bowen, Living with uncertainty: Genetic imprints of climate shifts in East Pacific anchovy (*Engraulis mordax*) and sardine (*Sardinops sagax*). *Mol. Ecol.* **13**, 2169–2182 (2004).

43. A. M. Vrooman, P. A. Paloma, J. R. Zweifel, Electrophoretic, morphometric, and meristic studies of subpopulations of northern anchovy, *Engraulis mordax*. *Cal. Fish Game* **67**, 39–51 (1981).

44. R. H. Parrish, D. L. Mallicoate, K. F. Mais, Regional variations in the growth and age composition of northern anchovy, *Engraulis mordax*. *Fish. Bull.* **83**, 483–496 (1985).

45. A. Audzijonyte, D. R. Barneche, A. R. Baudron, J. Belmaker, T. D. Clark, C. T. Marshal, J. R. Morrongiello, I. van Rijn, Is oxygen limitation in warming waters a valid mechanism to explain decreased body sizes in aquatic ecosystems? *Glob. Ecol. Biogeogr.* **28**, 64–77 (2018).

46. T. P. Boyer, J. I. Antonov, O. K. Baranova, C. Coleman, H. E. Garcia , A. Grodsky, R. A. Johnson, D. R. Locarnini, A. V. Mishonov, T. D. O'Brien, C. R. Paver, J. R. Reagan, D. Seidov, I. V. Smolyar, M. M. Zweng, World Ocean Database 2013. NOAA Atlas NESDIS 72 (2013); http://hdl.handle.net/11329/357.

47. J. K. Moore, S. C. Doney, J. A. Kleypas, D. M. Glover, I. Y. Fung, An intermediate complexity marine ecosystem model for the global domain. *Deep Sea Res. Part II Top Stud. Oceanogr.* **49**, 403–462 (2002).

48. K. E. Taylor, R. J. Stouffer, G. A. Meehl, An overview of CMIP5 and the experiment design. *Bull. Am. Meteorol. Soc.* **93**, 485–498 (2012).

49. C. Goute, E. Gaussier, A probabilistic interpretation of precision, recall and *F*-score, with implication for evaluation. *Adv. Inform. Retriev.* **3408**, 345–359 (2005).

50. A. Trujillo-Ortiz, R. Hernandez-Walls, gmregress: Geometric Mean Regression (Reduced Major Axis Regression) MATLAB file (2010); http://www.mathworks.com/matlabcentral/fileexchange/27918-gmregress.